Chemical Engineering Journal 158 (2010) 129–142

Contents lists available at ScienceDirect

Chemical Engineering Journal

journal homepage: www.elsevier.com/locate/cej

Development of mesoporous structure and high adsorption capacity of biomass-based activated carbon by phosphoric acid and zinc chloride activation

Tzong-Horng Liou*

Department of Chemical Engineering, Ming Chi University of Technology, 84 Gungjuan Rd., Taipei 24301, Taiwan

ARTICLE INFO

Article history:
Received 6 August 2009
Received in revised form 4 December 2009
Accepted 10 December 2009

Keywords:
Activated carbon
Mesoporous structure
Sugar cane bagasse
Sunflower seed hull
Chemical activation

ABSTRACT

This paper reports the preparation of activated carbon from two different types of agricultural biomass materials, sugar cane bagasse and sunflower seed hull, by phosphoric acid and zinc chloride activation. The experiments in this study vary the pre- and post-treatment procedures, the impregnation ratio of the activating agent, and the carbonization temperature. In recent years, the high surface area and high mesopore proportion of carbon have attracted a lot of attention for potential applications in the green resources such as hydrogen energy storage and carbon dioxide capture. However, the traditional methods for fabricating activated carbon produce a mainly microporous structure. The experimental results show that the activated carbon produced by base-leaching has a mostly mesoporous structure, which effectively enhances its adsorption capacity. The carbon materials obtained from zinc chloride activation of both sugar cane bagasse and sunflower seed hull have mesopore volumes as high as 1.07 and 0.95 cm^3/g, and mesopore contents of 81.2 and 74.0%, respectively. The surface area and pore volume of carbon produced using zinc chloride activation were higher than that produced using phosphoric acid activation. The total activation process of bagasse and hull occurs in three reaction stages. This study also presents a corresponding pyrolysis mechanism that agrees well with the experimental results. The proposed method of preparing mesoporous activated carbon is not complicated, and is suitable to bulk production.

1. Introduction

Activated carbon is an extremely versatile material with a high surface area. Due to its excellent adsorption capability, it is widely used in industrial wastewater and gas treatment [1,2]. The pore structure of activated carbon in conventional applications is mainly microporous. Recently, the potential use of activated carbon with a high proportion of mesoporous structures has attracted increasing attention because it possesses a high pore volume and a wide range of pore size. The mesoporous carbon materials are very suitable for use in large molecule adsorption, including battery capacitors, catalyst supports, biomedical engineering and adsorbents for bulky pollutants [3–5]. In the future, gasoline and diesel fuel for vehicles will probably be replaced for economy advantages. An important application of activated carbon is related to the gas storage for natural gas vehicles [6]. Moreover, researchers have paid significant attention to the use of carbon materials in hydrogen storage. Large pores are necessary for the fast mass transfer of adsorbate to the bulk of the carbon material [7]. Hence, the high surface area of activated carbon and its well-balanced micro/mesoporosity can provide an appropriate medium for energy storage. In particular, the CO_2 sorption of activated carbon plays an important role in reducing carbon emissions [8].

Sugar cane and sunflower are two of the most commonly cultivated plants in the world. Sugar cane bagasse is the waste material produced by sugar factories after sugar juice extraction. Sunflower seed hull is produced by oil extraction plants that manufacture bio-oil products. The production of sugar cane in Brazil, which is the largest global producer, totaled 425 million tons for the 2006/2007 season [9]. China and India are the two largest sugar cane producers in Asia. Together, these countries produced 437 million tons of sugar cane in 2008 [10]. On the other hand, global sunflower production reached 27 million tons in 2007 [11]. These two crops are abundantly available. Sugar cane and sunflower are also very good candidates for bio-ethanol and bio-diesel, which are used as alternative fuels [12,13]. The production of sugar cane and sunflower can be anticipated to increase significantly in the future. The observations above show that sugar, oil, and ethanol manufacturing processes produce a large amount of sugar cane bagasse and sunflower seed hull wastes each year. These wastes are usually burnt in the open or left in the field, and only a small portion is used as paper pulp or fuel. This creates disposal and pollution problems. The activated carbon obtained from these two agricultural wastes can provide useful, value-added products in the sugar factories, oil refineries, and related industries. Activated carbon for commercial utilization can be obtained by thermal treatment of low-cost and

* Tel.: +886 2 29089899; fax: +886 2 29083072.
E-mail address: thliou@mail.mcut.edu.tw.

1385-8947/$ – see front matter © 2009 Elsevier B.V. All rights reserved.
doi:10.1016/j.cej.2009.12.016

low ash content materials. Sugar cane bagasse just conforms to the rule for it is a low ash content and availability. In contrast, sunflower seed hull contains a high proportion of ash content. This study compares the two carbon products obtained from these two biomass sources.

Mesoporous activated carbon can be synthesized by many methods. Traditional methods use carbon precursors such as lignocellulosic materials, coals, and phenolic resins in the presence of transition metals, followed by a combination of carbonization and physical activation with stream or carbon dioxide, to obtain mesoporous activated carbon powder [14–16]. Shen et al. [17] used commercially activated carbon produced by steam activation with cerium oxide as a catalyst to prepare mesoporous carbon, and found that the catalyst restricted the formation of mesoporous structures at temperatures of 800–870 °C. Besides, some recent studies have developed mesoporous carbon with pores that can be controlled using mesoporous ceramic templates, such as SBA or MCM series [18,19]. Compared to the above methods, $ZnCl_2$ and H_3PO_4 are considered more effective and less expensive activating agents for producing mesoporous carbon [20,21]. Hu and Srinivasan [22] produced mesoporous activated carbon using coconut shells and palm seeds as starting materials, with simultaneous activation by $ZnCl_2$ and CO_2. They found that at a low $ZnCl_2$ concentration, the main pore characteristic is microporous; whereas at a high $ZnCl_2$ concentration, the main pore characteristic is mesoporous. Kennedy et al. [23] studied the H_3PO_4 activation of rice husk through precarbonization and chemical activation. They found that pores created at a higher activation temperature were enlarged or widened, leading to the formation of mesoporosity. Generally, activated carbon has a mesopore volume and a mesopore surface area in the range of 0.1–0.5 cm^3/g and 100–200 m^2/g, respectively [22]. However, for advanced applications, carbon materials should possess not only a high surface area, but also a high mesopore content. In particular, treating sugar cane bagasse and sunflower seed hull with an adequate base-leaching procedure enlarges or widens the micropore structure of the resulting carbon during the activation process. This, in turn, increases the mesopore surface area and mesopore volume. After activation, the carbon precursor must be washed with water to remove the chemical activating agent. However, traditional water-washing cannot effectively remove all chemical residues, and may result in the reduction of pore volume. In this case, acid-washing procedure is an adequate alternative [24].

Previous studies have already reported the preparation of mesoporous activated carbon from lignocellulosic materials by physical or chemical activation. However, the mesopore surface area and mesopore volume of these materials are not high enough, and many of the proposed approaches are complicated or require expensive equipments. In addition, there is a lack of information in the literature about activated carbon prepared from sugar cane bagasse and sunflower seed hull using H_3PO_4 or $ZnCl_2$ in a base-leaching or acid-washing process. This lack in existing literature is a motivation for the present study. The primary objective of this study is to compare activated carbon prepared from sugar cane bagasse and sunflower seed hull through chemical activation to produce a highly mesoporous activated carbon. The study investigates the effects of base-leaching, acid-washing, the impregnation ratio of activating agent, the kind of activating agent, and the carbonization temperature on the development of pore characteristics of activated carbon. Furthermore, the reactants and products are examined by several forms of analysis, including SEM, XRD, FTIR, ICP-MS, EA, TGA and a N_2-adsorption analyzer. The method of activated carbon preparation proposed in this study is not complicated, and well suited to mass production. Simultaneously, it is an effective way to enhance the mesopore surface area and mesopore volume of activated carbon.

2. Experimental

2.1. Materials

Sugar cane bagasse and sunflower seed hull were obtained from a sugar mill and a rural area, respectively. These two raw materials are respectively denoted as SCB and SSH hereafter. They were first washed thoroughly with distilled water to remove dust particles, and then dried at 100 °C, crushed, and sieved to obtain a uniform grain size approximately 10 mm long and 2 mm wide. ASTM standard test procedures were applied for ash content, volatile matter content and moisture content [25]. Fixed carbon was calculated from the difference. Table 1 lists the SCB and SSH contents in the proximate analysis. The elemental analysis section below illustrates the carbon, hydrogen, oxygen, and nitrogen contents of both raw materials. The weight percentages of ash content for SCB and SSH are 3.82 and 11.79 wt%, respectively. The ash content of SSH is three times as much as that of SCB.

2.2. Preparation of activation carbon

Preparing activated carbon from SCB and SSH can be divided into three stages, including base-leaching, activation, and acid-washing.

First, the water-rinsed bagasse and hull were leached with a 0.5 M NaOH (Merck & Co.) solution and boiled in a glass round-bottom flask at 100 °C for 1 h. The basic solution was drained and the remaining solid was washed with distilled water to remove the base. This process reduced the pH level to about 7. The material was then dried at 105 °C for 24 h.

Second, H_3PO_4 or $ZnCl_2$ of chemically pure quality (Merck & Co.) were used as activating agents. A known mass of activating agent was mixed with distilled water, and the bagasse and hull were then impregnated in the acidic solution. The impregnation ratio defined as the mass ratio of activating agent to dried solid, was 1–4. The impregnated samples were dried in a sand bath at high temperature to remove residual water, and then oven-dried for 24 h. A weighed amount of impregnated samples was then placed in a fixed bed reactor made of quartz. The reactor was purged with high-purity (99.95%) nitrogen gas (San-Fu Chem. Co.) at a high flow rate to avoid sample oxidation, and then the nitrogen flow was adjusted to the desired rate. The reactor was inserted into an electric furnace at reaction temperatures ranging from 400 to 800 °C, and the reaction continued for 1 h. The activated products were subsequently removed from the furnace and cooled to room temperature.

After activating the samples, 3 M hydrochloric acid was used to remove the phosphorous and zinc compounds. The activating agent and carbon mixtures were refluxed with hot acidic solution for 1 h. The remaining solid was then washed with distilled water until neutralization. The washed samples were dried at 105 °C for 24 h, and then ground to form a porous carbon powder.

Fig. 1 shows an experimental flow chart illustrating the methods above to help compare the effect of base-leaching and acid-washing on the surface characteristics of the samples. These tests were applied to several samples, as described below. Raw bagasse or

Table 1
Proximate analysis of sugar cane bagasse and sunflower seed hull.

Proximate analysis	SCB (wt%)	SSH (wt%)
Volatile matter	77.80	66.42
Ash	3.82	11.79
Fixed carbon	14.75	16.30
Moisture	3.63	5.49

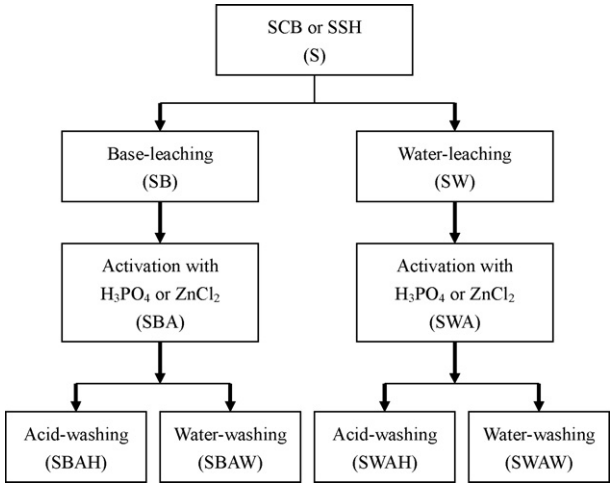

Fig. 1. Experimental flow chart expresses the methods used for treating the samples as base-leaching or acid-washing process.

hull only base-leached with NaOH, without chemical activation, is labeled as SB. Raw bagasse or hull that is first base-leached, and then activated with H_3PO_4 or $ZnCl_2$, and then washed with HCl solution, is labeled as SBAH. Samples in which acid-washing is replaced by a general water-washing are labeled as SBAW. Raw bagasse or hull washed with distilled water, activated with H_3PO_4 or $ZnCl_2$, and then washed with HCl solution is labeled as SWAH. Samples in which acid-washing is replaced by a general water-washing are labeled as SWAW.

2.3. Characterization

2.3.1. Measure of physical and chemical properties

To measure the amount of metallic impurities in the samples, the reactant and product were dissolved in a solution of HNO_3 and HF, and heated at 180 °C for 6 h. The amounts of metallic impurities in the solution were then determined with an inductively coupled plasma-mass spectrometer (ICP-MS) (Konton Plasmakon, model S-35). The amount of fundamental organic element for various treatment procedures was determined using a Heraeus elemental analyzer. The dried sample was powdered to a 325 mesh size (ASTM), and this powder was employed in the subsequent analysis.

The crystalline structures of the reactant and product were examined by an X-ray diffractometer (Siemens, Model D-500) using Cu-Kα radiation with a scan speed of 2.5° min^{-1}. Fourier transform infrared (FTIR) spectra were also obtained using a spectrometer to determine the composition of samples (Shimadzu, model FTIR-8300). The morphologies of the reactant and product were obtained with a scanning electron microscope (Topcon, model AST-150S).

2.3.2. Characteristics of N_2 and I_2 adsorption

The samples were characterized in terms of specific surface area, pore volume, and pore diameter. Samples were measured at −196 °C using the adsorption of nitrogen (Micrometric, model ASAP2010). The specific surface area of each specimen was calculated using the BET method [26]. This study assumes that the across-sectional area of a nitrogen molecule is 0.162 nm^2. The single point total pore volume was determined from the amount of adsorbed nitrogen expressed in liquid form at a relative pressure of approximately 0.95. The DR equation was applied to determine the micropore volume from the N_2-adsorption data [27]. This study assumes that micropores are less than 2 nm wide, mesopores are 2–50 nm wide, and macropores are more than 50 nm wide [28].

Adsorption tests were conducted using iodine adsorption capacity. The known amount of activated carbon was placed in a flask containing a 0.1 N iodine solution, and then shaken to maintain equilibrium for 24 h. After adsorption, the adsorbent was removed by filtration. The iodine adsorption capacity was determined from the titration of the filtrate with a $Na_2S_2O_3$ solution. The standard deviations of the BET surface area and iodine adsorption capacity are used as the basis for the error bars shown in the figures.

2.3.3. Thermogravimetric analysis

This study also used a Perkin-Elmer TGA7 thermogravimetric analyzer to conduct experiments on the activation of SCB and SSH impregnated with the activating agents [29]. For each experimental run, a known weight of 6 ± 0.5 mg was placed on a platinum sample pan. The samples were heated to 900 °C at a rate of 10 °C/min in a nitrogen atmosphere. This study defines the remaining amount of sample decomposed in nitrogen as W/W_o, where W_o and W represent the initial and instantaneous mass of the sample, respectively. The TG and DTG curves were recorded simultaneously as the temperature increased.

2.3.4. Calculation of activated carbon yield

The yield of activated carbon obtained from SCB and SSH for both H_3PO_4 and $ZnCl_2$-activated samples, was calculated from the weight of resultant activated carbons divided by the weight of dried raw materials.

3. Results and discussion

3.1. Effect of base and acid treatment on activation

Table 2 shows the effects of thermal decomposition and acid-washing on the purity of samples. Beside P and Zn elements, the raw materials (S) for both SCB and SSH samples have the highest concentration of metallic ingredients, including Mg, Ca, Fe, Na, K, and Cu. The SSH sample has a higher impurities content than the SCB sample. These metal elements are clearly reduced when samples are activated (SBAW or SBAH). It may be possible that the metals are carried by the vaporization of organic matter during carbonization [30]. When raw samples are base-leached, activated, and water-washed (SBAW), the element P in carbons activated by H_3PO_4 is much higher than in raw material samples. A similar trend is also observed that Zn impurity in carbons activated by $ZnCl_2$ is much higher than in raw material samples. This abrupt increase in the two impurities is because H_3PO_4 and $ZnCl_2$ remain in the sample after activation, and cannot be effectively removed by a simple water-washing step. When the activated samples were treated with a HCl solution (SBAH), the P and Zn elements were effectively reduced. Simultaneously, this process greatly decreased the concentration of other metals. This decrease in impurities may be due to metals dissolving in the acidic solution, and subsequent leaching and filtration. Experimental results show that the proportion of residual metals in the $ZnCl_2$-activated sample is lower than that in H_3PO_4-activated sample. In another words, Zn can be removed much more easily than P. This finding can be explained by the FTIR spectrum below, which shows that the phosphate and polyphosphate species incorporated into the carbon mixture through the C–O–P bands block the some of the pores in the carbon samples [31]. As a result, phosphorus compounds are not easily removed with washing. However, zinc salt is highly soluble in water, and is therefore easily removed in the washing stage [30]. The final purity of $ZnCl_2$-activated samples for both SCB and SSH is as high as 99.95%.

Table 3 lists the elemental analysis for raw bagasse and hull, base-leached, and activated samples. The major organic elements in raw materials (S) for both SCB and SSH are carbon and oxygen. The SSH sample has a higher ash content than the SCB sample. The

Table 2
Amount of metallic ingredients before and after the activation of samples.

	SCB (ppm)					SSH (ppm)				
	S[a]	SBAW[b]	SBAH[b]	SBAW[c]	SBAH[c]	S[a]	SBAW[b]	SBAH[b]	SBAW[d]	SBAH[d]
Mg	623	155	48	100	ND	3,950	86	ND	460	ND
Ca	635	330	125	ND	ND	12,300	470	350	200	120
Fe	477	106	ND	458	ND	1,480	95	ND	50	ND
Na	4089	504	251	265	69	190	390	330	320	160
K	778	97	39	ND	ND	5,330	190	ND	ND	ND
Mn	ND	ND	ND	ND	ND	49	ND	ND	ND	ND
Cu	29	39	ND	37	ND	59	ND	ND	40	ND
P	570	62100	36800	ND	ND	1,850	47800	27100	ND	ND
Zn	ND	ND	ND	28200	50	88	38	240	43300	150
Total	7201	63331	37263	29060	119	25,296	49069	28020	44370	430

ND means not detected.
[a] Samples were water-rinsed and un-heated.
[b] Samples were activated with H_3PO_4 at 400 °C.
[c] Samples were activated with $ZnCl_2$ at 500 °C.
[d] Samples were activated with $ZnCl_2$ at 600 °C.

inorganic components in the ash are mainly silica and metal impurities, which agrees with the results of other studies [32,33]. When the raw materials are base-leached (SB), the ash content clearly decreases. This reduction in ash content is due to the removal of silica in the sample. The silica reacts with the NaOH and forms sodium silicate (Na_2SiO_3) solution [34], and then is removed by filtration. When raw material samples were activated with H_3PO_4 or $ZnCl_2$ (SBAH), the percentage of carbon increased. However, hydrogen and oxygen exhibit the opposite trend. As generally recognized, hydrogen and oxygen can react with each other or with carbon. As a result, the gaseous volatiles are formed and are then released from the sample surface during pyrolysis [35]. The proportion of carbon in SCB-derived carbon samples is very close to that of SSH-derived carbon samples. For both SCB or SSH samples, the ash content in H_3PO_4-activated samples is higher than that in $ZnCl_2$-activated samples. This can be explained according by Table 2, which shows Zn salts are easily removed in the washing stage. However, P compounds are not easily removed due to the bonding of phosphorus and carbon in the activated sample.

Fig. 2 plots the BET surface area and iodine adsorption capacity of samples as a function of the base-leaching or acid-washing procedure. Experimental results show that the base-leaching and acid-washing have obvious effect on the adsorption performance of samples. For all samples, the iodine adsorption capacity increases as the BET surface area increases. The BET surface areas (do not show in the figure) of both SCB and SSH for the raw material samples (S) are 0.60 and 0.06 m^2/g, and that of base-leached samples (SB) are 1.56 and 0.59 m^2/g, respectively. The base-leached samples can remove the ash and leave a number of tiny pores, and therefore increase the surface area of carbon precursor. Fig. 2(a) and (b) shows the results of SCB and SSH carbon samples for H_3PO_4 activation using various treatment procedures. The BET surface areas are the lowest for non-base and non-acid treated samples (SWAW). The surface area obtained mainly comes from the vaporization of organic matter during the activation process, leaving the porous surface. The surface area of the SCB-derived carbon obtained from SWAW process is 886 m^2/g, which is very close to the value of 881 m^2/g reported by Castro et al. [36] in their study of the H_3PO_4 activation of sugar cane bagasse at 400 °C. When SCB or SSH samples are treated with SWAH process, the surface areas of activated carbon increase significantly. This can be explained by the metallic ingredient analysis in Table 2, which shows that the residual activating agents adhered to the interior of the carbon samples after activation block the pores. This leads to a reduction in the sample's adsorption capacities. However, the activating agent can be removed by an acid-washing process, which increases the surface area. When SCB or SSH samples are base-leached, activated, and water-washed (SBAW), the BET surface area and iodine adsorption capacity are abruptly enhanced. The base-leaching process (SBAW) enhances the surface area more than the acid-washing process (SWAH). The element analysis in Table 3 shows that the raw bagasse and hull contain the ash content. The inorganic components in the ash probably prevent porosity evolution by blocking pore entrances during the activation process [37]. Hence, when the ash is removed by an adequate base-leaching step, this increases the surface area of the activated carbon. Soleimani and Kaghazchi [38] reported that activated carbon with a high ash content is undesirable because it reduces the mechanical strength and adsorption capacity of the carbon, which is consistent with the present experimental results. The BET surface area and iodine adsorption capacity reach their maximum when the activated SCB and SSH samples are base-leached and acid-washed (SBAH). This indicates that combining both base-leaching and acid-washing procedures creates a dual influence after activation. Fig. 2(c) and (d) illustrate the BET surface area and iodine adsorption capacity of $ZnCl_2$-activated samples obtained from before and after treatment procedures. The effect of $ZnCl_2$ activation on the sample's surface characteristics is similar to that of H_3PO_4 activation, which can be enhanced by acid-washing or base-leaching processes.

Table 3
Elemental composition and ash content before and after the activation of samples.

	SCB (wt%)				SSH (wt%)			
	S[a]	SB[b]	SBAH[c]	SBAH[d]	S[a]	SB[b]	SBAH[c]	SBAH[e]
C	45.03	44.88	63.68	84.45	41.60	45.81	62.74	86.51
H	6.88	6.05	4.67	3.56	5.20	5.58	4.22	2.68
O[f]	44.03	48.38	27.72	11.48	40.49	47.31	29.87	10.34
N	0.24	0.06	0.08	0.06	0.92	0.14	0.12	0.22
Ash	3.82	0.63	3.85	0.45	11.79	1.16	3.05	0.25

[a] Samples were water-rinsed and un-heated.
[b] Samples were base-leached and un-heated.
[c] Samples were activated with H_3PO_4 at 400 °C.
[d] Samples were activated with $ZnCl_2$ at 500 °C.
[e] Samples were activated with $ZnCl_2$ at 600 °C.
[f] By difference.

The experimental results of this study show that base-leaching offers several potential benefits: (i) reducing the ash content in the samples to avoid obstructing the pore development, (ii) helping the activating agent enter the interior of the carbon tissue after removing the ash, which increases the contact area between the activating agent and the carbon precursor, and (iii) allowing the base solution to decompose or soften the organic matter in the raw material [39], which facilitates the pyrolysis of bagasse or hull into carbon during activation. For these reasons, base-leaching can increase the surface area of activated carbons. The surface areas show an increase

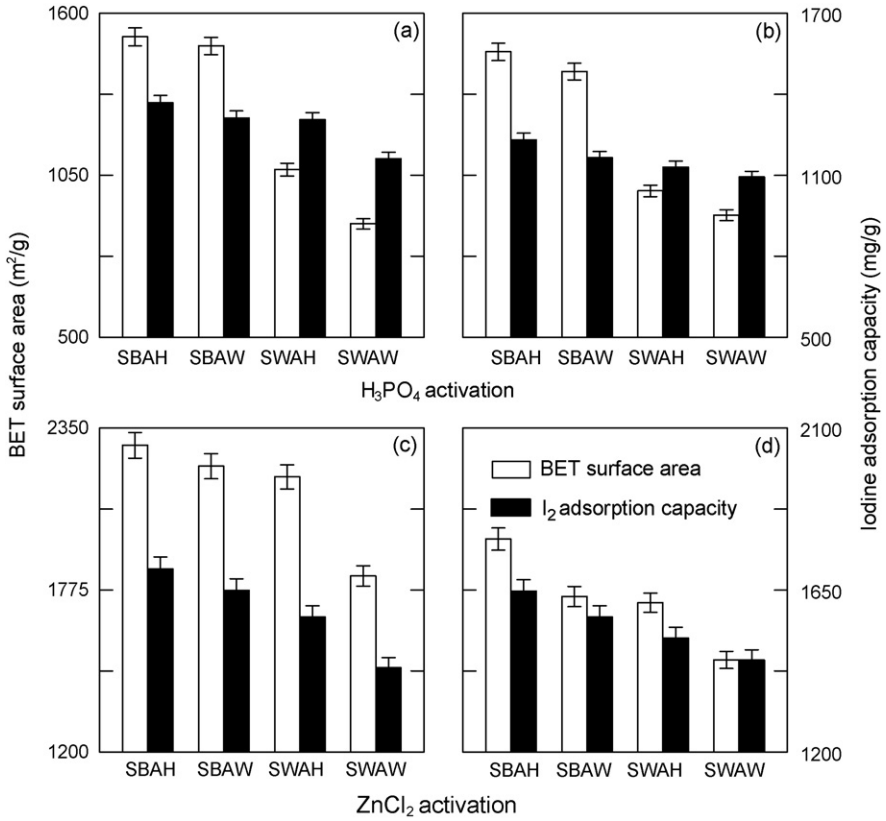

Fig. 2. Effect of base and acid treatment on the surface area and iodine adsorption capacity of samples at impregnation ratio of 2: (a) SCB-based carbon with H_3PO_4 activation at 400 °C, (b) SSH-based carbon with H_3PO_4 activation at 400 °C, (c) SCB-based carbon with $ZnCl_2$ activation at 500 °C, and (d) SSH-based carbon with $ZnCl_2$ activation at 600 °C.

of 480–605 m^2/g by H_3PO_4 activation and 225–390 m^2/g by $ZnCl_2$ activation, respectively. Yun et al. [37], who studied the carbonization of rice straw as a biomass precursor, reported similar findings. They found that removing the inorganic component in the raw straw creates new pores and voids, which increase the surface area and pore volume. According to the experimental results in Fig. 2, the surface area and adsorption capacity of carbon can be enhanced using a combination of base-leaching and acid-washing processes. Hence, the remaining experiments in the study are conducted with both procedures.

3.2. Effect of H_3PO_4 on activation reaction

Fig. 3 shows the BET surface area and iodine adsorption capacity of H_3PO_4-activated samples with different activation temperatures and impregnation ratios. Fig. 3(a) and (b) shows the effect of impregnation ratio on the surface characteristics of SCB and SSH samples. As the impregnation ratio increases from 1 to 2, the adsorption capacities are enhanced. This is due to an increase in the contact area between the raw material and the activating agent. This, in turn, increases the release of volatiles and increases the pore surface area. However, further increasing the impregnation ratio from 2 to 4 causes a decrease in adsorption capacity. This observation is probably due to the contraction of pore structure caused by the thermal breakdown of phosphate esters at a high ratio of activating agent to carbon precursor [36]. Like the impregnation ratio samples above, Fig. 3(c) and (d) shows the surface area and adsorption capacity for both SCB and SSH under various activation temperatures. These figures indicate that the highest adsorption capacity occurs at the activation temperature of 500 °C. Increasing the activation temperature increases the thermal decomposition rate, and therefore increases the surface area of carbon. However, when the activation temperature exceeds 500 °C, the resulting surface area decrease may be due to contraction or collapse of pores at high temperature [40]. Under the same conditions, activated carbon from sugar cane bagasse exhibits a higher BET surface area and iodine adsorption capacity than carbon prepared from sunflower seed hull. This indicates that the performance of the resulting carbon depends on the raw material used as the precursor. This discrepancy probably arises from the different constituents inherent in each precursor, including cellulose, hemicellulose and lignin. These organic matters can lead to different pore evolution mechanism in the carbon [38,41]. The optimum surface areas for SCB and SSH samples for H_3PO_4 activation at 500 °C are 1611 and 1543 m^2/g, respectively.

3.3. Effect of $ZnCl_2$ on activation reaction

Fig. 4 illustrates the effect of $ZnCl_2$ activation on the BET surface area and iodine adsorption capacity of samples. The adsorption behavior of $ZnCl_2$-activated samples is the same as that of H_3PO_4-activated samples. The highest surface area and adsorption capacity of samples occur at an activation temperature and impregnation ratio of 500 °C and 2, respectively. Yorgun et al. [25] studied the $ZnCl_2$ activation of Paulownia wood. They pointed out that $ZnCl_2$ worked as a dehydration regent during carbonization. This result leads to the charring and aromatization of the carbon skeleton and creation of the porous structure. On the other hand, $ZnCl_2$ can also restrict the tar formation. When the reaction temperature is lower than 500 °C, more volatiles are released by increasing the reaction temperature, and the surface area increases. However, a reaction temperature greater than 500 °C, this decrease in surface area of carbon can be attributed to the heat shrinking [42]. Lua and Yang [43] reported a similar trend that increasing the impregnation ratio

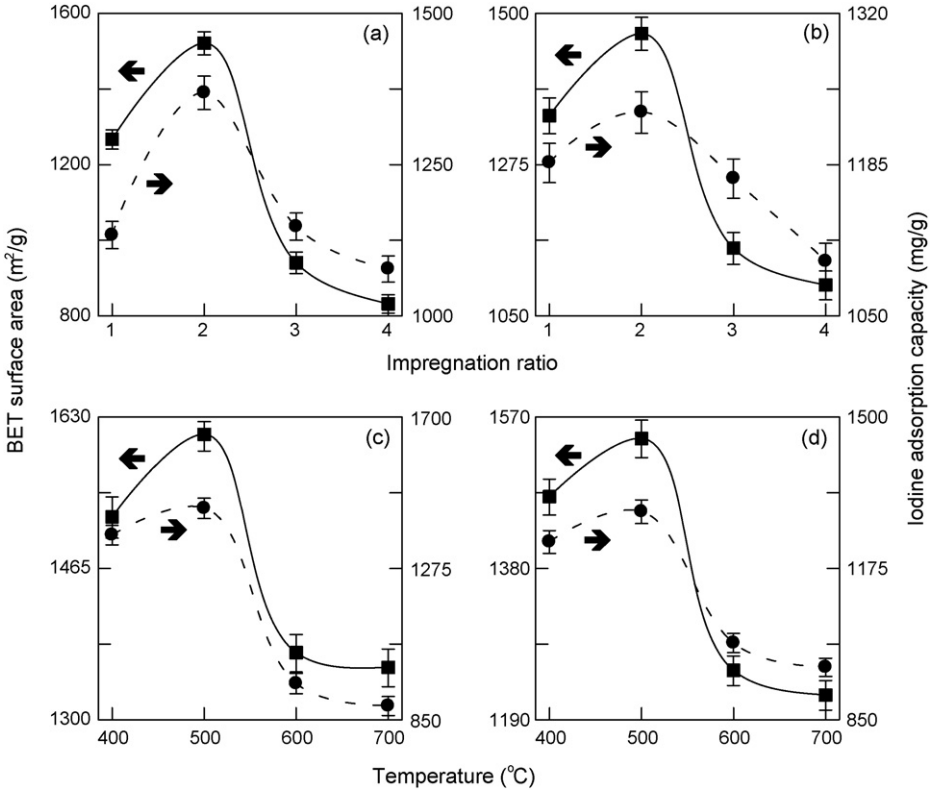

Fig. 3. Effect of H_3PO_4 activation on the surface area and iodine adsorption capacity of samples: (a) SCB-based carbon at 400 °C, (b) SSH-based carbon at 400 °C, (c) SCB-based carbon at impregnation ratio of 2, and (d) SSH-based carbon at impregnation ratio of 2.

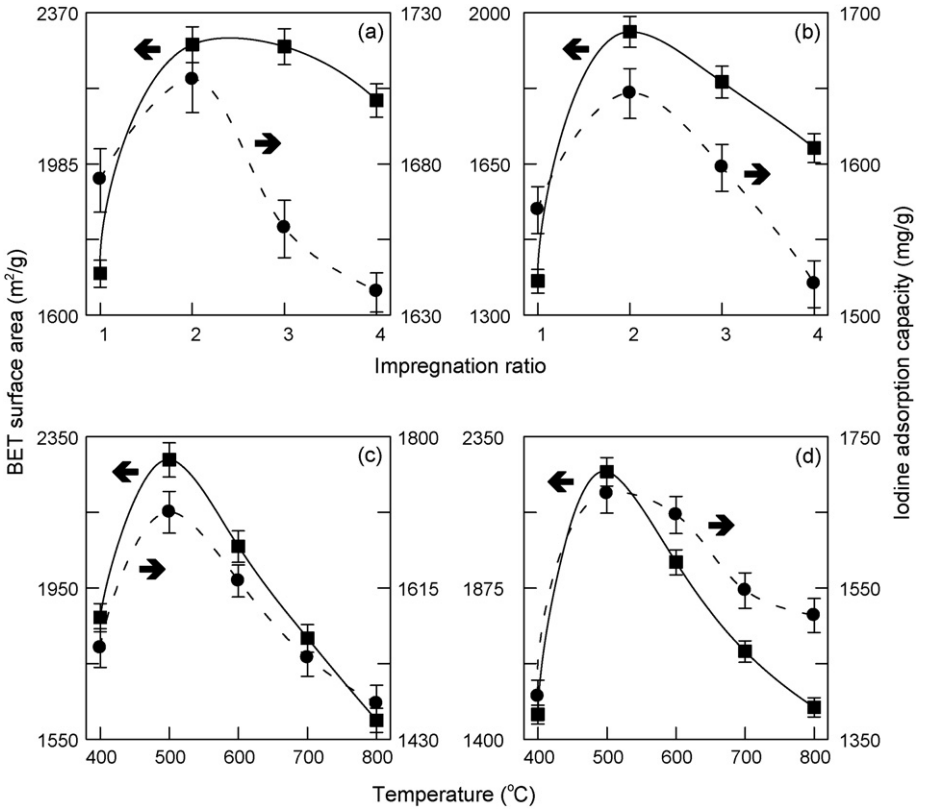

Fig. 4. Effect of $ZnCl_2$ activation on the surface area and iodine adsorption capacity of samples: (a) SCB-based carbon at 500 °C, (b) SSH-based carbon at 600 °C, (c) SCB-based carbon at impregnation ratio of 2, and (d) SSH-based carbon at impregnation ratio of 2.

of $ZnCl_2$ from 0.25 to 1.50 increases the pore surface area of carbon. A comparison of Figs. 3 and 4 shows that $ZnCl_2$-activated carbon always has greater surface areas and adsorption capacities than H_3PO_4-activated carbon. The optimum surface areas of SCB and SSH carbons for $ZnCl_2$ activation at 500 °C are 2289 and 2240 m^2/g, respectively.

3.4. Pore structure analysis

Fig. 5 plots the nitrogen adsorption–desorption isotherms of H_3PO_4-activated samples at reaction temperatures ranging from 400 to 700 °C. The curve trends for volume adsorbed from SCB and SSH are vary similar. When raw material samples are un-treated (SWAW samples), the adsorption curves are Type I isotherms that do not display an apparent desorption hysteresis loop, in accordance with IUPAC classification [44]. This adsorption behavior implies that the carbon materials are highly microporous. When samples are base- and acid-treated at various activation temperatures, the isotherms display an abrupt increase in adsorbed volume at a low relative pressure (P/P_o). This adsorption behavior exhibits a Type I isotherm as characteristic of microporous structure [45]. As the relative pressure increases, the nitrogen uptake increases across the entire pressure range. Furthermore, as the relative pressure increases to 0.4, the isotherms exhibit apparent hysteresis loops. This adsorption behavior exhibits a Type IV isotherm as characteristic of mesoporous structure. Therefore, the activated carbon obtained from various activation temperatures show both microporous and mesoporous structures [22]. The samples' nitrogen adsorption capacities also change with activation temperature, and reach their maximum at 500 °C.

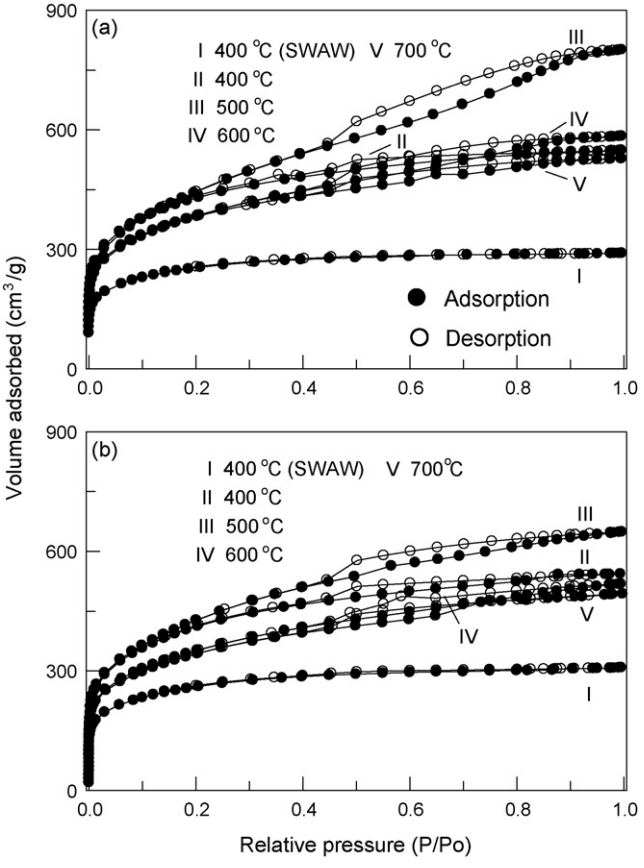

Fig. 5. Adsorption–desorption isotherm of H_3PO_4 activation samples at impregnation ratio of 2: (a) SCB-based carbon and (b) SSH-based carbon.

Table 4 shows the specific surface area and pore volume of carbon samples obtained from H_3PO_4 activation at various temperatures. When the SCB and SSH carbons are obtained neither acid-treated nor base-treated (SWAW), they exhibit significantly lower surface areas. The two carbon samples have higher microporous volume than mesoporous volume. However, the total pore volumes of the carbon are only 0.448 and 0.475 cm^3/g, respectively. A similar property is also observed by other studies [36] that activated carbon obtained from H_3PO_4 activation of non-base-treated sugar cane bagasse, had the main pore characteristic of microporosity. Both the pore volume and specific surface area increase when the two raw materials are activated and followed by acid and base treatments (SBAH). This indicates that removing ash and residual activating agent effectively enhances the pore volume and surface area. Experimental results also show that the carbon obtained from SBAH process produces a higher mesopore volume and mesopore surface area. As mentioned earlier, base-leaching raw material samples decreases the ash content and leaves a number of tiny pores. Simultaneously, NaOH decomposes the tissue of the carbon precursor, which also creates some new pores and voids. The activating agent permeates these tiny pores or voids, which increase the contact area between the activating agent and the carbon precursor. Consequently, this promotes the release of volatiles from the carbon structure and widens the micropores in the original carbon structure, converting them into mesopores. In addition, the activating agent probably deposits on the interior of the pores after water-washing, as Fig. 2 indicates. This may lead to pore contraction and microporosity formation. However, acid-washing removes the activating agent enlarging the micropores and increasing mesoporosity. An increase in the activation temperature produces optimum surface area and pore volume values. The highest pore volumes, which occur at 500 °C, are 1.233 and 0.999 cm^3/g for SCB- and SSH-derived carbon, respectively. The optimum temperature of 500 °C has also been reported by other studies, which prepared activated carbon from lignocellulosic materials such as cherry stones using H_3PO_4 activation [46]. Experimental results show that activated carbon prepared from sugar cane bagasse possesses a higher pore volume and surface area than sunflower seed hull. The trends of total pore volume and surface area are reflected in the mesopore pore volume and mesopore surface area. Consequently, both SCB and SSH carbon samples produced at 500 °C posses mesopore volumes of 0.802 and 0.696 cm^3/g, and mesopore surface areas of 1068 and 975 m^2/g, respectively. The mesopore contents of 500 °C H_3PO_4-activated carbon approach 65.0 and 69.7% for SCB and SSH, respectively. The mesopore contents exceed the expected proportion of conventional microporous carbon. The average pore diameters of H_3PO_4-activated samples for both SCB and SSH range from 2.2 to 3.1 nm and 2.2 to 2.6 nm, respectively. The carbon yield decreases as the reaction temperatures increases. A higher reaction temperature releases more volatiles and therefore produces a lower yield. The yield values of base- and acid-treated carbon (SBAH) are lower than un-treated carbon (SWAW). This is because base-leaching removes a portion of the organic matter in the precursor (according to SEM observation), and this causes a decrease in the carbon yield. Further, SSH-derived samples yield more carbon than SCB-derived samples. This can be explained by the fact that the mass loss of organic matter in SCB is higher than that of SSH after base-leaching. This, in turn, causes a reduction in the carbon yield of the SCB samples.

Fig. 6 illustrates the pore characteristics of samples activated with $ZnCl_2$ at various activation temperatures. These isotherms resemble a combination of Type I and Type IV isotherms. All samples show a broad knee and a pronounced desorption hysteresis loop. The slope of the plateaus in these isotherms gradually increases as increasing the relative pressure. These results indicate that the pore structure of $ZnCl_2$-activated carbon is mainly

Table 4
Pore volume, surface area, and activated carbon yield for the samples activated by H_3PO_4.

	SCB (°C)					SSH (°C)				
	400[a]	400[b]	500[b]	600[b]	700[b]	400[a]	400[b]	500[b]	600[b]	700[b]
V_t (cm^3/g)	0.448	0.846	1.233	0.900	0.814	0.475	0.838	0.999	0.798	0.761
V_{mic} (cm^3/g)	0.273	0.336	0.129	0.210	0.287	0.258	0.313	0.191	0.213	0.219
V_{meso} (cm^3/g)	0.162	0.489	0.802	0.568	0.445	0.200	0.474	0.696	0.506	0.461
V_{meso}/V_t (%)	36.16	57.80	65.04	63.11	54.67	42.11	56.56	69.67	63.41	60.58
S_{BET} (m^2/g)	886	1521	1611	1373	1357	915	1470	1543	1252	1221
S_{meso} (m^2/g)	260	717	1068	773	623	313	694	975	687	645
D_p (nm)	2.02	2.23	3.06	2.62	2.40	2.07	2.28	2.59	2.55	2.49
Yield (%)	46.42	25.42	24.87	23.84	21.68	46.65	33.14	32.25	32.20	30.65

V_t = total pore volume, V_{mic} = micropore volume, V_{meso} = mesopore volume, S_{BET} = BET surface area, S_{meso} = mesopore surface area, D_p = average pore diameter calculated as $4V/A$, where A is the BET surface area and V is the single point total pore volume.
[a] Samples were treated with SWAW process.
[b] Samples were treated with SBAH process.

Table 5
Pore volume, surface area, and activated carbon yield for the samples activated by $ZnCl_2$.

	SCB (°C)					SSH (°C)				
	500[a]	400[b]	500[b]	600[b]	700[b]	600[a]	400[b]	500[b]	600[b]	700[b]
V_t (cm^3/g)	1.082	1.026	1.358	1.311	1.091	0.896	0.776	1.318	1.116	1.030
V_{mic} (cm^3/g)	0.298	0.419	0.237	0.153	0.202	0.273	0.384	0.292	0.283	0.182
V_{meso} (cm^3/g)	0.667	0.545	1.046	1.065	0.836	0.541	0.312	0.952	0.790	0.762
V_{meso}/V_t (%)	61.65	53.12	77.03	81.24	76.63	60.38	40.21	72.23	70.79	73.98
S_{BET} (m^2/g)	1825	1872	2289	2060	1817	1527	1478	2240	1956	1676
S_{meso} (m^2/g)	1197	852	1567	1544	1233	983	492	1421	1199	1124
D_p (nm)	2.27	2.19	2.37	2.55	2.40	2.14	2.10	2.35	2.28	2.46
Yield (%)	41.08	21.29	19.27	19.07	17.60	43.50	29.62	29.11	27.32	25.04

V_t = total pore volume, V_{mic} = micropore volume, V_{meso} = mesopore volume, S_{BET} = BET surface area, S_{meso} = mesopore surface area, D_p = average pore diameter calculated as $4V/A$.
[a] Samples were treated with SWAW process.
[b] Samples were treated with SBAH process.

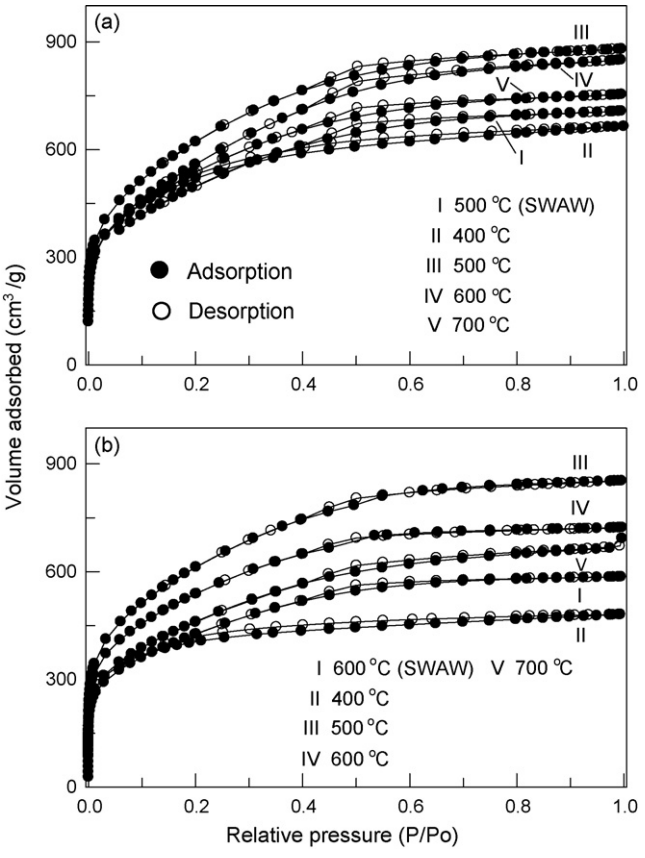

Fig. 6. Adsorption–desorption isotherm of $ZnCl_2$ activation samples at impregnation ratio of 2: (a) SCB-based carbon and (b) SSH-based carbon.

mesoporous. At the same activation temperature, the nitrogen adsorption capacities of un-treated samples are clearly lower than that of base-treated samples. Nitrogen adsorption capacity reaches its highest value at an activation temperature of 500 °C. Table 5 illustrates the pore volume, surface area, and activated carbon yield for the samples activated by $ZnCl_2$. The pore structure of carbon prepared without base-leaching and acid-washing exhibits a mixture of both micropore and mesopore. When the activated carbon samples are acid-washed and base-leached, the mesopore volume and mesopore surface area increase further. These results suggest that removal of ash transforms the micropores into mesopores due to pore widening. The SCB and SSH samples have the highest pore volumes of 1.358 and 1.318 cm^3/g at 500 °C, respectively. The SCB and SSH carbon samples produced at 500 °C possess mesopore volumes of 1.046 and 0.952 cm^3/g and mesopore surface areas of 1567 and 1421 m^2/g, respectively. The proportion of mesopore volume in SCB and SSH samples activated with $ZnCl_2$ at 500 °C approach the values of 77.0 and 72.2%. These values are higher than those of conventional activated carbon. Moreover, the mesopore content of the SCB sample reaches a value of 81.2% at 600 °C.

$ZnCl_2$-activated samples possess a higher mesopore volume and mesopore surface area than H_3PO_4-activated samples. This is because acid-washing removes $ZnCl_2$ much more easily than H_3PO_4, reducing the possibility of activating agent deposition on the pores and sample surface. This, in turn, increases the mesopore volume and mesopore surface area. The ratio of micropores to mesopores in activated carbon can be adjusted by changing the before and after treatment procedure, the type of activating agent, and the activation temperature. The average pore diameters of $ZnCl_2$-activated samples range from 2.2 to 2.6 for SCB and 2.1 to 2.5 nm for SSH. The activated carbon yield of samples decreases as the reaction temperature increases, as can be seen in Table 5. The SSH-derived samples yield more carbon than the SCB-derived

samples. These results are similar to those of the H_3PO_4 activation procedure (Table 4).

Fig. 7 shows the pore size distribution determined using the BJH method for SCB and SSH samples activated with H_3PO_4 and $ZnCl_2$ [17]. For un-treated samples (SWAW), the carbon obtained from H_3PO_4 activation shows a weak peak at a pore diameter of about 3.5 nm. A narrow peak of carbon obtained from $ZnCl_2$ activation for the un-treated process approaches 3.2 nm. When samples are treated with base-washing and acid-washing (SBAH), the peak position shifts to 3.5 nm after $ZnCl_2$ activation, and reaches a value of 3.9 nm for H_3PO_4-activated samples. This indicates that many micropores are enlarged, and the structure eventually becomes mesoporous.

3.5. Analysis of physical properties

Fig. 8 shows the XRD patterns of raw materials and activated carbon obtained from H_3PO_4 and $ZnCl_2$ activation at various reaction temperatures. In the raw SCB and SSH samples, a broad peak appearing at $2\theta = 22.5^\circ$ is a typical silica characteristic, which can be attributed to the presence of disordered cristobalite [47]. The peak disappears when raw materials are base-treated and activated with H_3PO_4 and $ZnCl_2$ at all temperatures, indicating the removal of ash. Two broad peaks appear at approximately $2\theta = 25^\circ$ and 45° after activation with H_3PO_4 and $ZnCl_2$, indicating the formation of turbostratic structure of disordered carbon. The peaks at $2\theta = 45^\circ$ became stronger as the reaction temperature increases. This indicates that carbon tends to crystallize at an elevated temperature. The peak intensity for samples using the $ZnCl_2$ activation procedure is higher than that using the H_3PO_4 activation procedure. Kennedy et al. [48] reported that peaks at $2\theta = 45^\circ$ are due to the creation of pores by the decomposition of carbon along the direction of the graphic structures. This produces relatively well-organized aromatic carbon that is more stable than amorphous-like carbon.

Fig. 9 shows the FTIR spectroscopy of samples used to study the chemical compositions of the raw materials and carbon products. The spectra obtained form SCB and SSH have many similar features because they are lignocellulosic materials [43]. For the raw material samples of both SCB and SSH, a wide band located in the range of 3200–3400 cm^{-1} is a consequence of O-H groups and adsorbed water [49]. The band at 2918 cm^{-1} is due to C-H vibration. The band at 1737 cm^{-1} is related to the stretching of C=O groups. The band at 1646 cm^{-1} may be due to the stretch vibrations of C=C bonds in olefinic structures. The two bands at 1505 and 1425 cm^{-1} are the skeletal C=C vibrations of aromatic rings. The stretching vibrations of $-CH_3$ at 1378 cm^{-1} are related to methyl structures. The adsorption between 1000 and 1350 cm^{-1} may be assigned to C–O vibrations. The O–H band is located at 665 cm^{-1}. The spectra of activated carbon are different from those of raw materials. Many bands disappear, indicating the vaporization of organic matters. All of the carbon samples show a wide band at about 3425 cm^{-1}, which is due to the O-H vibrations of hydroxyl groups. When SCB and SSH are activated with $ZnCl_2$, the band located at about 1604 cm^{-1} is attributable to C=C vibrations. The bands located at 1165 and 864 cm^{-1} are due to C–O and C–H vibrations [43]. When SCB and SSH are activated with H_3PO_4, the bands that appear between 900 and 1200 cm^{-1} may be attributed to the presence of phosphorus species in the samples [48]. The peak at 1175 cm^{-1} can be assigned to C–O stretching vibrations in a C–O–P linkage. The shoulder at 1053 cm^{-1} may represent a chain of P–O–P vibrations.

Fig. 10 shows electron microscope images of raw materials and carbon samples obtained from SCB and SSH. Fig. 10(a) and (b) shows the outer epidermis and inner surface of original sugar cane bagasse, respectively. The outer epidermis of the bagasse has a

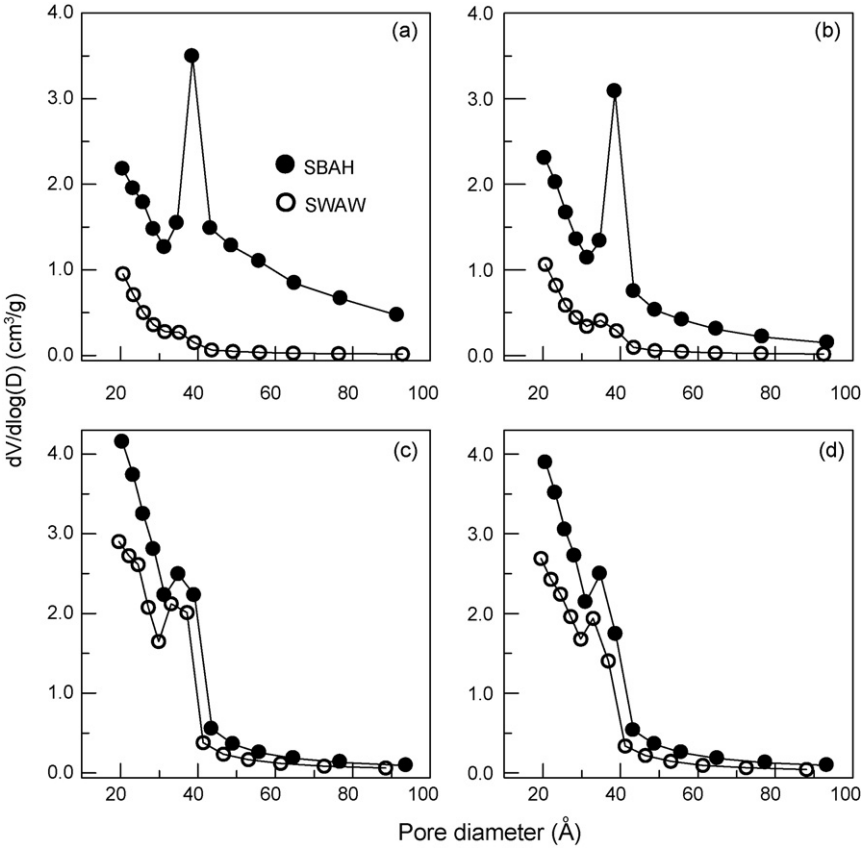

Fig. 7. Pore size distribution of samples treated with SWAW or SBAH process: (a) SCB-based carbon with H_3PO_4 activation at 400 °C, (b) SSH-based carbon with H_3PO_4 activation at 400 °C, (c) SCB-based carbon with $ZnCl_2$ activation at 500 °C, and (d) SSH-based carbon with $ZnCl_2$ activation at 600 °C.

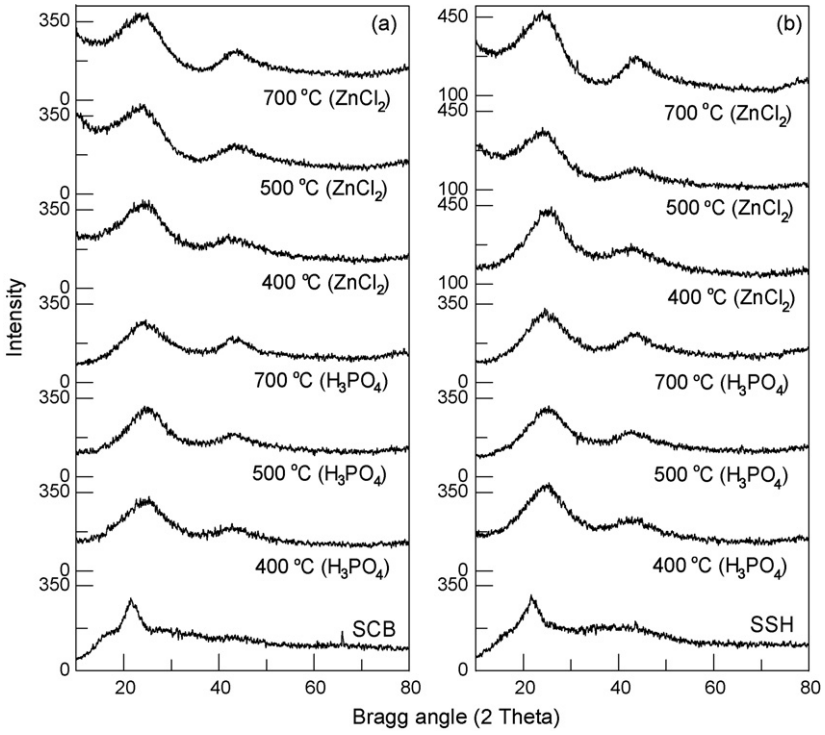

Fig. 8. X-ray diffractogram of samples activated with H_3PO_4 or $ZnCl_2$: (a) SCB-based carbon and (b) SSH-based carbon.

smooth and pitted surface. The inner surface of the bagasse is a long and narrow strip. Fig. 10(c) shows the inner surface of base-leached bagasse. The surface characteristic of the sample is slightly altered by the base-leaching process, and appears clear-cut, indicating that a portion of the organic tissue of the SCB sample is dissociated after the base-leaching procedure. Rao et al. [50] reported that soaking raw bagasse in a NaOH solution can remove the lignin content, which is similar to the present experimental results. Fig. 10(d) shows that the morphology of SCB-derived carbon powder activated with H_3PO_4 is a long column. However, activated carbon produced by $ZnCl_2$ activation has an irregular shape, as Fig. 10(e) indicates. Fig. 10(f) shows the outer epidermis of a sunflower seed hull, which is orderly tubular tissue. Fig. 10(g) shows the inner surface of sunflower seed hull. The morphology of hull is similar to that of the SCB (Fig. 10(b)), which is a long narrow strip. Fig. 10(h) shows the outer epidermis of base-leached hull. The surface of the outer epidermis is peeled off and contains a number of rectangular tissues, indicating the removal of part of the hull's organic matter. Fig. 10(i) and (j) shows the morphology of carbon powders obtained from SSH and activated with H_3PO_4 and $ZnCl_2$, respectively. These figures show that the two activation procedures do not significantly affect the surface morphology of the resulting carbons, which has an irregular grain shape. However, $ZnCl_2$-activated carbon has a few small pores distributed within the solid.

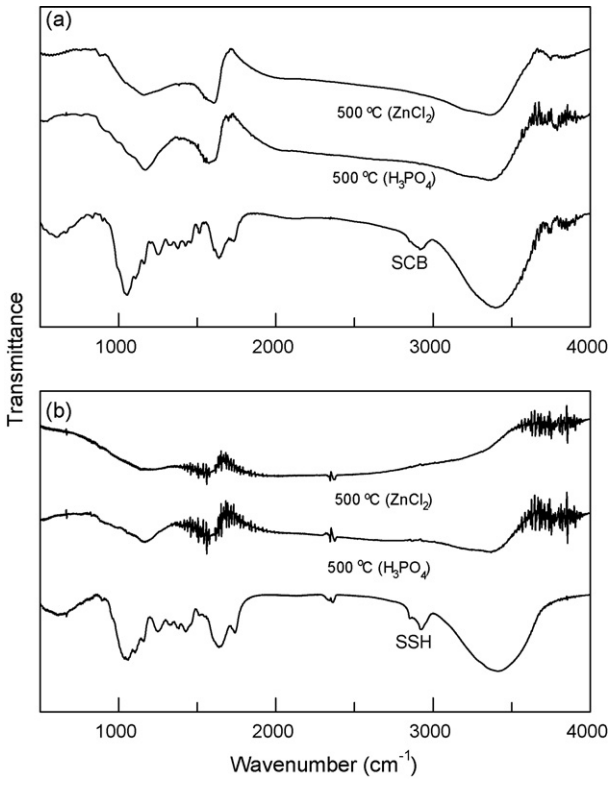

Fig. 9. FTIR spectrogram of samples activated with H_3PO_4 or $ZnCl_2$: (a) SCB-based carbon and (b) SSH-based carbon.

3.6. Analysis of thermal characteristic and reaction path

Fig. 11 shows the TG and DTG curves of samples activated with H_3PO_4 and $ZnCl_2$ at various impregnation ratios. Fig. 11(a) and (b) shows the TGA curves of H_3PO_4-activated SCB and SSH, respectively. The TG curves exhibit three temperature zones. This mirrors the fact that the activation of bagasse and hull with H_3PO_4 occurs in three main stages. At a constant activation temperature, the mass loss caused by specimen decomposition increases as the impregnation ratio increases. In the first stage, the small amount of mass loss in the TG curves as the temperature reaches ~300 °C is due to the pyrolysis of organic matter in the carbon precursor. The mass loss of the heating curves in the second stage ranged from 300 to 550 °C, which is smaller than that in the first stage. This loss may be associated with a transition period in the activation. A significant mass loss occurs in the third stage, as the temper-

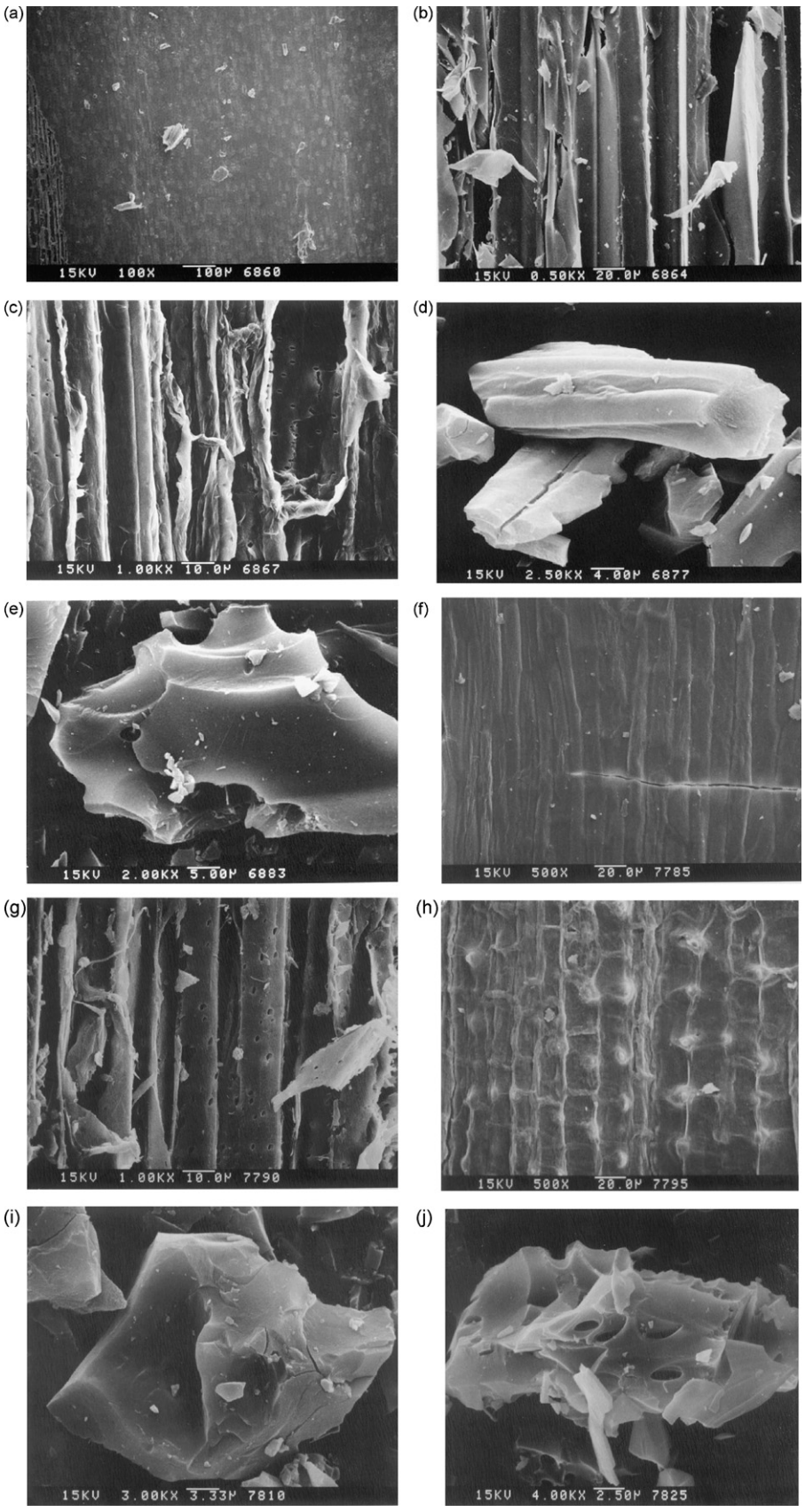

Fig. 10. Scanning electron microscope images of samples: (a) and (b) outer epidermis and inner surface of SCB, (c) inner surface of base-leached SCB, (d) and (e) SCB-based carbon powders by H_3PO_4 and $ZnCl_2$ activation, respectively, (f) and (g) outer epidermis and inner surface of SSH, (h) outer epidermis of base-leached SSH, (i) and (j) SSH-based carbon powders by H_3PO_4 and $ZnCl_2$ activation, respectively.

ature increases from 550 to 900 °C. The DTG curves in Fig. 11(a) and (b) shows that two peaks appear in each heating curve. The temperature of the first peak increases as the impregnation ratio increases, while the temperature of the second peak decreases as the impregnation ratio increases. Furthermore, the height of the peak, which is associated with the instantaneous rate of pyrolysis, also increases as the impregnation rate increases. This indicates that the reaction rate can be enhanced by increasing the amount of chemical activating agent. Experimental results also show that SCB samples have slightly lower activation temperatures than SSH samples.

Fig. 11(c) and (d) shows the TGA plots of $ZnCl_2$-activated SCB and SSH obtained at various impregnation ratios of activating agent. The mass loss in these samples occurs in three temperature zones, namely ~200, 200–450 and 450–800 °C. Qian et al. [35] reported that three stages of thermal decomposition were observed in the chemical activation of cattle-manure compost with $ZnCl_2$, which is similar to the present experimental observations. The DTG curves reveal two peak temperatures for SCB and SSH samples activated at various impregnation ratios. The temperature of the first peak increases as the impregnation ratio increases, while the temperature of the second peak increases as the impregnation ratio decreases. These results are similar to those of the H_3PO_4 activation procedure. Thermogravimetric analysis shows that the thermal decomposition mechanism of SCB is very similar to that of SSH for both H_3PO_4 and $ZnCl_2$ activation. However, SCB activation has a higher instantaneous rate of thermal decomposition and a lower peak temperature, indicating that the SCB activation occurs more easily than SSH activation. A comparison of H_3PO_4-activated carbon and $ZnCl_2$-activated carbon shows that $ZnCl_2$ activation produces a lower peak temperature and shorter duration of pyrolysis, as well as a higher instantaneous rate of thermal decomposition. These observations also suggest that the $ZnCl_2$ activation occurs more quickly and easily than H_3PO_4 activation.

Due to the complexity of this activation, researchers do not fully understand the pyrolysis paths of activation. The different pore characteristics of carbon activated by either H_3PO_4 or $ZnCl_2$ activation depend on the process conditions and the composition of raw materials. However, this study reveals the main mechanism for this activation. Essentially, the organic constituent of SCB and SSH is a biopolymer including cellulose, hemi-cellulose and lignin [38,51]. The hemi-cellulose and lignin are probably embedded in the interior of the cellulose matrix [40]. Thermogravimetric analysis (Fig. 11) shows that a small amount of mass loss appears in the initial stage of both $ZnCl_2$ and H_3PO_4 activation. This indicates that the two chemicals first attack the organic matter in the bagasse or hull [52]. In this case, chemical reactions between the activating agent and biomass cause the decomposition or depolymerization of celluloses and lignin into intermediates with a smaller molar mass. Simultaneously, gaseous volatiles such as H_2O, CO, CO_2, CH_4 and aldehydes are released from the sample surface [35]. This is consistent with FTIR spectra (Fig. 9) observations, in which many bands disappear after activation, indicating the volatilization of organic matter. Jagtoyen and Derbyshire [40] reported that the mass loss occurring during the primary activation is due to a loss of aliphatic character, which simultaneously leads to an increase in aromaticity by rearranging the atomic structure. As the activation temperature increases, the mass loss in the second stage begins to transform gently. The main characteristic of the reaction at this stage is probably due to an expansion of the volumetric structure of the samples, which in turn reduces the release of volatiles [36]. The XRD curves in Fig. 8 reflect the same trends in the volumetric expansion, in that peak intensity increases as the reaction temperature increases. This indicates an increase in crystalline size or

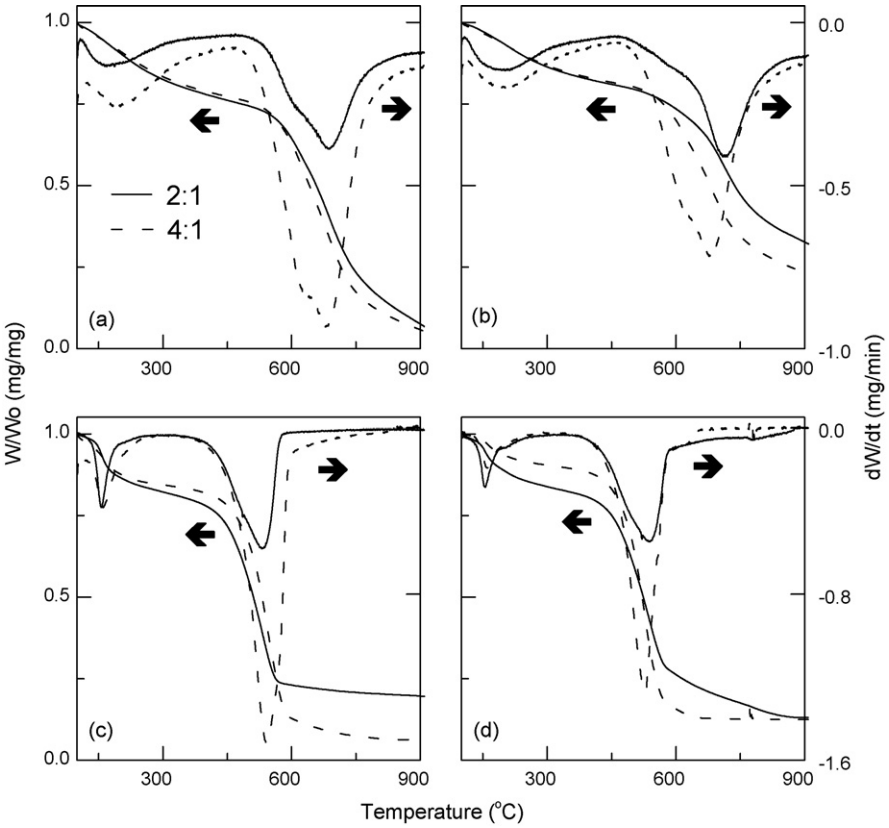

Fig. 11. TG and DTG thermogram of samples at impregnation ratios of 2 and 4: (a) SCB-based samples with H_3PO_4 activation, (b) SSH-based samples with H_3PO_4 activation, (c) SCB-based samples with $ZnCl_2$ activation, and (d) SSH-based samples with $ZnCl_2$ activation.

aromatic structure of carbon when reaction temperature increases. Olivares-Marin et al. [53] further showed that the mass loss deceleration at 250–500 °C for the carbon precursors activated with H_3PO_4 may be attributed to the formation of phosphate esters via cellulose phosphorylation. These observations indicate that a cross-linking reaction combines carbon, hydrogen, and oxygen in the carbon precursors. Simultaneously, cross-linking reactions begin to control the activation of samples rather than decomposition and depolymerization reactions [46]. This situation increases the aromatization of the carbonized char and also improves porosity. In the initial period of the second stage reaction, the pores are formed in a short retention time and therefore are mostly microporous. As the reaction temperature increases, the carbon structure continues to expand, which leads to an increase in mesoporosity.

However, as the activation temperature continues to rise, Fig. 11 shows a significant mass loss in the third stage of both H_3PO_4 and $ZnCl_2$ activation. The observation can be explained by the fact that the boiling point of H_3PO_4 is 407 °C [46] and the chemical transformation of H_3PO_4 into P_2O_5 occurs in the temperature range of 580–585 °C [54]. The melting point of $ZnCl_2$ is 283 °C [35] and the vaporization of $ZnCl_{2(l)}$ occurs in the temperature range of 480–550 °C [55]. Therefore, this mass loss can be attributed to the release of residual activating agents and a few volatiles. Due to the cross-linking of the phosphate esters in carbon precursor during H_3PO_4 activation process should increase the pyrolysis temperature. Thermogravimetric analysis shows that H_3PO_4 activation requires a longer heating duration than $ZnCl_2$ activation to increase the thermal degradation temperature. As a result, the severe gasification of volatiles for both H_3PO_4 and $ZnCl_2$ activation at high reaction temperatures cause a sintering reaction or bond cleavage, which in turn causes pore shrinkage or collapse. The observations above are consistent with the analysis results of pore characteristics in Figs. 5 and 6, which indicate that the development of porosity of carbon reaches its maximum value at a carbonization temperature of 500 °C. Lua and Yang [43] further pointed out that the decreasing porosity of carbon activated with $ZnCl_2$ at higher reaction temperatures is due to the sintering of volatiles, which causes the pore structure to shrink. When the activation is complete, activated carbon with a porous structure can be obtained after the final process of water- or acid-washing.

4. Conclusions

Using sugar cane bagasse and sunflower seed hull as raw materials, this study reports the preparation of activated carbon with a highly mesoporous surface area. Both H_3PO_4 and $ZnCl_2$ serve as chemical activating agents. The starting raw materials, before and after treatment processes, and conditions employed for carbon synthesis, strongly affect the final pore structure and the adsorption behavior of the resulting carbon. The proposed base-leaching procedure can effectively enhance the surface area and pore volume of samples. The removal of ash from the activated carbon results in pore widening and the development of mesoporosity. The largest pore volume and surface area of activated carbon prepared from SCB and SSH samples using H_3PO_4 and $ZnCl_2$ activation processes occur at 500 °C and an impregnation ratio of 2. Simultaneously, the mesopore volume and mesopore surface area are also accompanied by an increase in the largest amounts. The surface areas of the activated carbon are as high as 1611 and 2289 m^2/g for SCB, and 1543 and 2240 m^2/g for SSH, for H_3PO_4 and $ZnCl_2$ activation, respectively. The SCB-based carbon shows a slightly higher surface area and pore volume than SSH-based carbon. Thermogravimetric analysis shows that the thermal decomposition mechanism of SCB-based samples is similar to that of SSH-based samples. However, SCB-based activation occurs more easily than SSH-based activation. The reaction mechanism for both H_3PO_4 and $ZnCl_2$ activation can be illustrated experimentally. The proposed method of preparing activated carbon using an adequate base-leaching process is inexpensive, simple and well-suited to mass production, especially for application in sustainable fuel and the adsorption of bulky pollutant.

Acknowledgement

The author expresses thanks to the National Science Council of Taiwan for its financial support under Project No. NSC 94-2214 – E131 – 003.

References

[1] D. Kalderis, D. Koutoulakis, P. Paraskeva, E. Diamadopoulos, E. Otal, J.O. del Valle, C. Fernández-Pereira, Adsorption of polluting substances on activated carbons prepared from rice husk and sugarcane bagasse, Chem. Eng. J. 144 (2008) 42–50.
[2] O. Ioannidou, A. Zabaniotou, Agricultural residues as precursors for activated carbon production—a review, Renew. Sust. Energ. Rev. 11 (2007) 1966–2005.
[3] Y.J. Kim, B.J. Lee, H. Suezaki, T. Chino, Y. Abe, T. Yanagiura, K.C. Park, M. Endo, Preparation and characterization of bamboo-based activated carbons as electrode materials for electric double layer capacitors, Carbon 44 (2006) 1592–1595.
[4] H. Tamai, U. Nobuaki, H. Yasuda, Preparation of Pd supported mesoporous activated carbons and their catalytic activity, Mater. Chem. Phys. 114 (2009) 10–13.
[5] R.V. Ramanujan, S. Purushotham, M.H. Chia, Processing and characterization of activated carbon coated magnetic particles for biomedical applications, Mater. Sci. Eng. C: Bio. Sci. 27 (2007) 659–664.
[6] M.J. Prauchner, F. Rodríguez-Reinoso, Preparation of granular activated carbons for adsorption of natural gas, Micropor. Mesopor. Mater. 109 (2008) 581–584.
[7] C. Vix-Guterl, E. Frackowiak, K. Jurewicz, M. Friebe, J. Parmentier, F. Béguin, Electrochemical energy storage in ordered porous carbon materials, Carbon 43 (2005) 1293–1302.
[8] B. Guo, L. Chang, K. Xie, Adsorption of carbon dioxide on activated carbon, J. Nature Gas Chem. 15 (2006) 223–229.
[9] M.C.R. Halmeman, S.N.M. de Souza, P.T. Oyama, Potential and costs for the production of electrolytic hydrogen in alcohol and sugar cane plants in the central and south regions of Brazil, Int. J. Hydrog. Energy 33 (2008) 6858–6864.
[10] G. Kostka, C. Polzin, J. Scharrer, The future of sugar cane in China and India—supply constraints and expansion potential, Appl. Energy 86 (2009) S100–S107.
[11] C. Pickardt, S. Neidhart, C. Griesbach, M. Dube, U. Knauf, D.R. Kammerer, R. Carle, Optimisation of mild-acidic protein extraction from defatted sunflower (*Helianthus annuus* L.) meal, Food Hydrocolloids 23 (2009) 1966–1973.
[12] M. Balat, M. Balat, Recent trends in global production and utilization of bio-ethanol fuel, Appl. Energy 86 (2009) 2273–2282.
[13] G. Antolín, F.V. Tinaut, Y. Briceño, V. Castaño, C. Pérez, A.I. Ramírez, Optimisation of biodiesel production by sunflower oil transesterification, Bioresour. Technol. 83 (2002) 111–114.
[14] K. Nakagawa, S.R. Mukai, K. Tamura, H. Tamon, Mesoporous activated carbons from phenolic resins, Chem. Eng. Res. Des. 85 (2007) 1331–1337.
[15] E. Lorenc-Grabowska, G. Gryglewica, Adsorption characteristics of Congo red on coal-based mesoporous activated carbon, Dyes Pigment 74 (2007) 34–40.
[16] H. Tamai, U. Nobuaki, H. Tasuda, Preparation of Pd supported mesoporous activated carbons and their catalytic activity, Mater. Chem. Phys. 114 (2009) 10–13.
[17] W. Shen, J. Zheng, Z. Qin, J. Wang, Preparation of mesoporous carbon from commercial activated carbon with steam activation in the presence of cerium oxide, J. Colloid Interface Sci. 264 (2003) 467–473.
[18] M.J. Lázaro, L. Calvillo, E.G. Bordejé, R. Moliner, R. Juan, C.R. Ruiz, Functionalization of ordered mesoporous carbons synthesized with SBA-15 silica as template, Micropor. Mesopor. Mater. 103 (2007) 158–165.
[19] C.N. Mbileni, F.F. Prinsloo, M.J. Witcomb, N.J. Coville, Synthesis of mesoporous carbon supports via liquid impregnation of polystyrene onto a MCM-48 silica template, Carbon 44 (2006) 1476–1483.
[20] Z. Zhu, A. Li, L. Yan, F. Liu, Q. Zhang, Preparation and characterization of highly mesoporous spherical activated carbons from divinylbenzene-derived polymer by $ZnCl_2$ activation, J. Colloid Interface Sci. 316 (2007) 628–634.
[21] M. del Mar Gómez-Tamayo, A. Macías-García, M.A. Díez, E.M. Cuerda-Correa, Adsorption of Zn(II) in aqueous solution by activated carbons prepared from evergreen oak (*Quercus rotundifolia* L.), J. Hazard. Mater. 153 (2008) 28–36.
[22] Z. Hu, M.P. Srinivasan, Mesoporous high-surface-area activated carbon, Micropor. Mesopor. Mater. 43 (2001) 267–275.
[23] L.J. Kennedy, J.J. Vijaya, K. Kayalvizhi, G. Sekaran, Adsorption of phenol from aqueous solutions using mesoporous carbon prepared by two-stage process, Chem. Eng. J. 132 (2007) 279–287.
[24] D. Lozano-Castello, M.A. Lillo-Rodenas, D. Cazorla-Amoros, A. Linares-Solano, Preparation of activated carbons from Spanish anthracite. I. Activation by KOH, Carbon 39 (2001) 741–749.

[25] S. Yorgun, N. Vural, H. Demiral, Preparation of high-surface area activated carbons from Paulownia wood by $ZnCl_2$ activation, Micropor. Mesopor. Mater. 122 (2009) 189–194.
[26] S. Brunauer, P.H. Emmett, E. Teller, Adsorption of gases in multimolecular layers, J. Am. Chem. Soc. 60 (1938) 309–319.
[27] M.M. Dubinin, Fundamentals of the theory of adsorption in micropores of carbon adsorbents: characteristics of their adsorption properties and microporous structures, Carbon 27 (1989) 457–467.
[28] G.H. Oh, C.R. Park, Preparation and characteristics of rice-straw-based porous carbons with high adsorption capacity, Fuel 81 (2002) 327–336.
[29] T.H. Liou, Kinetics study of thermal decomposition of electronic packaging material, Chem. Eng. J. 98 (2004) 39–51.
[30] T.H. Liou, S.J. Wu, Characteristics of microporous/mesoporous carbons prepared from rice husk under base- and acid-treated conditions, J. Hazard. Mater. 171 (2009) 693–703.
[31] S. Timur, I.C. Kantarli, E. Ikizoglu, J. Yanik, Preparation of activated carbons from Oreganum stalks by chemical activation, Energy Fuels 20 (2006) 2636–2641.
[32] D. Kalderis, S. Bethanis, P. Paraskeva, E. Diamadopoulos, Production of activated carbon from bagasse and rice husk by a single-stage chemical activation method at low retention times, Bioresour. Technol. 99 (2008) 6809–6816.
[33] M.J. Fernández Llorente, J.E. Carrasco García, Comparing methods for predicting the sintering of biomass ash in combustion, Fuel 84 (2005) 1893–1900.
[34] T. Li, T. Wang, Preparation of silica aerogel from rice hull ash by drying at atmospheric pressure, Mater. Chem. Phys. 112 (2008) 398–401.
[35] Q. Qian, M. Mochida, H. Tatsumoto, Preparation of activated carbons from cattle-manure compost by zinc chloride activation, Bioresour. Technol. 98 (2007) 353–360.
[36] J.B. Castro, P.R. Bonelli, E.G. Cerrella, A.L. Cukierman, Phosphoric acid activation of agricultural residues and bagasse from sugar cane: influence of the experimental conditions on adsorption characteristics of activated carbons, Ind. Eng. Chem. Res. 39 (2000) 4166–4172.
[37] C.H. Yun, Y.H. Park, G.H. Oh, C.R. Park, Contribution of inorganic components in precursors to porosity evolution in biomass-based porous carbons, Carbon 41 (2003) 2009–2012.
[38] M. Soleimani, T. Kaghazchi, Agricultural waste conversion to activated carbon by chemical activation with phosphoric acid, Chem. Eng. Technol. 30 (2007) 649–654.
[39] T.H. Usmani, T.W. Ahmad, A.H.K. Yousufzai, Preparation and liquid-phase characterization of granular activated-carbon from rice husk, Bioresour. Technol. 48 (1994) 31–35.
[40] M. Jagtoyen, F. Derbyshire, Activated carbons from yellow poplar and white oak by H_3PO_4 activation, Carbon 36 (1998) 1085–1097.
[41] M.M. Yeganeh, T. Kaghazchi, M. Soleimani, Effect of raw materials on properties of activated carbons, Chem. Eng. Technol. 29 (2006) 1247–1251.
[42] K. Mohanty, M. Jha, B.C. Meikap, M.N. Biswas, Preparation and characterization of activated carbons from Terminalia Arjuna nut with zinc chloride activation for the removal of phenol from wastewater, Ind. Eng. Chem. Res. 44 (2005) 4128–4138.
[43] A.C. Lua, T. Yang, Characteristics of activated carbon prepared from pistachionut shell by zinc chloride activation under nitrogen and vacuum conditions, J. Colloid Interface Sci. 290 (2005) 505–513.
[44] S.J. Gregg, K.S.W. Sing, Adsorption, Surface Area and Porosity, Second ed., Academic Press, London, 1982.
[45] T.H. Liou, Evolution chemistry and morphology during the carbonization and combustion of rice husk, Carbon 42 (2004) 785–794.
[46] M. Olivares-Marín, C. Fernández-González, A. Macías-García, V. Gómez-Serrano, Porous structure of activated carbon prepared from cherry stones by chemical activation with phosphoric acid, Energy Fuels 21 (2007) 2942–2949.
[47] T.H. Liou, F.W. Chang, J.J. Lo, Pyrolysis kinetics of acid-leached rice husk, Ind. Eng. Chem. Res. 36 (1997) 568–573.
[48] L.J. Kennedy, J.J. Vijaya, G. Sekaran, Effect of two-stage process on the preparation and characterization of porous carbon composite from rice husk by phosphoric acid activation, Ind. Eng. Chem. Res. 43 (2004) 1832–1838.
[49] Y. Guo, D.A. Rockstraw, Physicochemical properties of carbons prepared from pecan shell by phosphoric acid activation, Bioresour. Technol. 98 (2007) 1513–1521.
[50] M. Rao, A.V. Parwate, A.G. Bhole, Removal of Cr^{6+} and Ni^{2+} from aqueous solution using bagasse and fly ash, Waste Manage. 22 (2002) 821–830.
[51] A. Demirbas, Effect of temperature on pyrolysis products from four nut shells, J. Anal. Appl. Pyrolysis 76 (2006) 285–289.
[52] P.T. Williams, A.R. Reed, Development of activated carbon pore structure via physical and chemical activation of biomass fibre waste, Biomass Bioenergy 30 (2006) 144–152.
[53] M. Olivares-Marin, C. Fernandez-Gonzalez, A. Macias-Garcia, V. Gomez-Serrano, Thermal behavior of lignocellulosic material in the presence of phosphoric acid. Influence of the acid content in the initial solution, Carbon 44 (2006) 2330–2356.
[54] D. Montané, V. Torné-Fernández, V. Fierro, Activated carbons from lignin: kinetic modeling of the pyrolysis of Kraft lignin activated with phosphoric acid, Chem. Eng. J. 106 (2005) 1–12.
[55] E. Oniyama, P.G. Wahlbeck, Application of transpiration theory to TGA data: calcium carbonate and zinc chloride, Thermochim. Acta 250 (1995) 41–53.